The hydrodynamic lift of a slender, neutrally buoyant fiber in a wall bounded shear flow at small Reynolds number

Johnson Dhanasekaran[1] and Donald L. Koch[2]†

[1]Sibley School of Mechanical and Aerospace Engineering,Cornell University, Ithaca, New York 14853, USA

[2]Smith School of Chemical and Biomolecular Engineering,Cornell University, Ithaca, New York 14853, USA

(Received xx; revised xx; accepted xx)

The hydrodynamic lift velocity of a neutrally buoyant fiber in a simple shear flow near a wall is determined for small, but non-zero, fiber Reynolds number, illustrating the role of non-sphericity in lift. The rotational motion and effects of fiber orientation on lift are treated for fiber positions that induce and do not induce solid-body wall contacts. When the fiber does not contact with the wall its lift velocity can be obtained in terms of the Stokes flow field by using a generalized reciprocal theorem. The Stokes velocity field is determined using slender-body theory with the no-slip velocity at the wall enforced using the method of images. To leading order the lift velocity at distances large compared with the fiber length and small compared with the Oseen length is found to be $0.0303\rho\dot{\gamma}^2 l^2 a/(\mu \ln[\frac{2l}{a}])$, where l and a are the fiber half-length and radius, ρ is the density, $\dot{\gamma}$ is the shear rate and μ is the viscosity of the fluid. When the fiber is close enough to the wall to make solid-body contact during its rotational motion, a process known as pole vaulting coupled with inertially induced changes of fiber orientation determines the lift velocity. The order of magnitude of the lift in this case is larger by a factor of l/a than when the fiber does not contact the wall and it reaches a maximum of $0.006\rho\dot{\gamma}^2 l^3/(\mu \ln[\frac{l}{a}])$. These results are used to illustrate how particle shape can contribute to separation methods such as those in microfluidic channels or cross-flow filtration processes.

Key words:

1. Introduction

Hydrodynamic lift is the motion of a particle transverse to the streamlines of the imposed flow and the direction of any body force on the particle. It results from the stresses on the particle caused by fluid inertia when the particle Reynolds number is finite. Hydrodynamic lift plays an important role in separation processes such as microfluidic focusing (see Masaeli *et al.* 2012) and cross-flow filtration(see Drew *et al.* 1991). While there is extensive literature analysing the lift on a spherical particle(see Saffman 1965; McLaughlin 1991, 1993; Cherukat & McLaughlin 1994; Drew 1988), relatively little is known about the lift on non-spherical particles. To gain insight into the role of non-

† Email address for correspondence: dlk15@cornell.edu

sphericity we derive the lift velocity of a neutrally buoyant high aspect ratio cylindrical fiber in a wall-bounded simple shear flow at small, but finite, particle Reynolds number $\mathrm{Re} = \rho\dot{\gamma}l^2/\mu$. Here, l is the fiber half-length, ρ is the fluid density, $\dot{\gamma}$ is the shear rate and μ is the viscosity of the fluid. In addition to providing a large contrast to the commonly studied spherical shape, the choice of fibers allows the use of slender-body theory to describe the flow induced by the fiber, facilitating a quasi-analytical treatment.

Much is known about the hydrodynamic lift on a spherical particle in simple shear flow at small, but non-zero, particle Reynolds number. This lift requires breaking the symmetry of the flow to allow cross-streamline motion. This is achieved by either a body force acting on the particle parallel to the flow direction or a nearby wall. Saffman (1965) calculated the lift on a sphere in an unbounded shear flow induced by a body force parallel to the streamlines for the case when relative velocity due to the body force is much smaller than the imposed shear velocity, $\dot{\gamma}a$, where a is the sphere radius. McLaughlin (1991) generalized this investigation to cover all ratios of the relative velocity and shear velocity. The nature of the analysis for the lift on a particle in the presence of a wall depends on the relative magnitude of the separation from the wall h^* and the Oseen length $L_0 = [\mu/(\rho\dot{\gamma})]^{1/2}$. McLaughlin (1993) studied hydrodynamic lift on spheres at separations comparable to or larger than the Oseen length. This outer analysis involves a singular perturbation analysis that includes a viscous dominated inner region spanning distances of $O(a)$ from the particle and an outer region at separations of $O(L_0)$ where inertial and viscous effects are comparable. However, when the particle is closer to the wall than the Oseen length, the inertial effects can be treated as a regular perturbation from the Stokes flow solution. This inner analysis was carried out by Cherukat & McLaughlin (1994) to evaluate the lift force on spheres. The special case of this result, corresponding to no force along the streamlines, can be used in conjunction with appropriate Stokes flow resistance functions to evaluate the lift velocity of a neutrally buoyant particle. The lift velocity is expected to exhibit very different qualitative and quantitative behaviour due of non-sphericity. This will be especially pronounced in the inner analysis where the fiber geometry has close interaction with the wall. Thus, the focus of this study will be on fibers in the inner region, $h^* \ll L_O$, where a regular perturbation analysis in terms of Re is applicable.

The study of the lift on non-spherical particles is very limited compared to the literature available on the lift on spheres. One of the earliest treatments on non-sperical shapes was carried out by Harper & Chang (1968) who calculated lift force on three dimensional bodies in unbounded shear flow. Shin *et al.* (2009) studied the lift on a fiber due to a body-force induced relative velocity and a weak, unbounded shear flow. Numerical studies of the lift-induced trajectories of an elliptical particle have been carried out by Feng *et al.* (1994) in Couette and Poiseuille flows, considering both neutrally buoyant and sedimenting particles. Qi (1999) has numerically studied the lift of rectangular particles. However, there is no analytical treatment of the lift on a force-free fiber. Neither is there any literature available for the hydrodynamic lift of a particle with high aspect ratio (fiber) as a function of the distance from the wall in the presence of a shear flow.

Hydrodynamic lift can play an important role in separating particles of different types and separating particles from fluid. A common method of separating particles in microchannels is to allow hydrodynamic lift to cause different types of particles to migrate to different positions in the channel. A bifurcation in the channel can then be used to harvest the desired particle type. While such separations have conventionally been based on particle size, Masaeli *et al.* (2012) have demonstrated experimentally that particle shape plays an important role. In cross-flow filtration, a suspension of particles flows

through a channel with porous walls, while fluid filtrate is drawn out through the walls. A major advantage of cross-flow filtration is that the shearing motion helps to limit the formation of a filter cake of particles at the porous membrane surface. Belfort and Drew and co-investigators (see Drew *et al.* 1991; Belfort *et al.* 1994; Drew 1988) have argued that hydrodynamic lift, in addition to hydrodynamic diffusion and Brownian diffusion, helps to limit the particle concentration at the membrane surface. Many targets for such separation processes have non-spherical prolate shapes, including biological particles such as bacteria and viruses as well as cellulose fibers of current interest in the production of biofuels. Thus understanding non-spherical particles' hydrodynamic behaviour will go a long way in improving their filtration in industrial and laboratory settings.

The order of magnitude of the lift velocity of a neutrally buoyant sphere in a shear flow near a wall at small Reynolds number can be understood in a simple way. The characteristic Stokes fluid velocity disturbance in the vicinity of a sphere is $\dot{\gamma}a$. However, any cross-stream motion of a particle in Stokes flow would violate Stokes flow reversibility. Thus, the lift velocity is the result of fluid inertia, which is quantified by the particle Reynolds number $\mathrm{Re}_a = \rho\dot{\gamma}a^2/\mu$. The lift velocity of a sphere is thus proportional to $\dot{\gamma}a\mathrm{Re}_a = \rho\dot{\gamma}^2a^3/\mu$.

One can estimate some properties of nonspherical particles in low Reynolds number flows as those associated with an equivalent sphere. For example, a common means of estimating the drag on an object in Stokes flow is as the drag on a circumscribing sphere. However, we will see that the lift on a slender fiber at small but finite Reynolds number differs in order of magnitude from that of a circumscribing sphere and furthermore the dependence of lift on separation from the wall is qualitatively different for fibers and spheres. One important reason for this difference is the role that fiber rotation plays in the lift. A fiber rotates in a periodic motion through a Jeffery orbit (see Jeffery 1922) spending most of its time near the flow direction and a shorter time flipping through other orientations. Since the fluid velocity disturbance made when the fiber is nearly aligned with the flow direction is much smaller than while it is flipping, its lift behaviour does not resemble that of any equivalent sphere.

Since the lift velocity of a fiber depends on its orientation, a specification of the time dependent orientation of the fiber is required to predict its spatial migration. In Stokes flow, a fiber rotates periodically in time in one of a set of Jeffery orbits parametrized by the orbit constant C. At small but finite Reynolds numbers, Subramanian & Koch (2005) showed that the fiber spirals gradually through orbits and eventually rotates in the $C = \infty$ orbit corresponding to orientations within the flow-gradient plane. We will consider the time-averaged lift that occurs when the fiber has been in the shear flow long enough to reach the $C = \infty$ orbit.

The lift velocity of a fiber that does not make contact with the wall but is within the viscous dominated region, i.e., $l < h^* \ll L_0$, can be determined using a regular perturbation analysis for $\mathrm{Re} \ll 1$. In carrying out this analysis we will use the generalised reciprocal theorem to avoid the expensive evaluation of the order Reynolds flow field. This enables the $O(\mathrm{Re})$ fiber velocity to be related to a volume integral involving the Stokes fluid velocity field and a comparison field driven by a fiber with a unit force acting perpendicular to the wall. The Stokes flow field consists of the imposed shear flow and a disturbance flow created by the fiber and its hydrodynamic interaction with the wall. The disturbance velocity field due to the particle is represented by a line of Stokeslets distributed along the particle axis. The force distribution on the particle is evaluated by solving the integral equations of the slender-body theory, developed by Batchelor (1970), under the simplifying assumption of high aspect ratio. The hydrodynamic interaction of the fiber with the wall is included by using, for each Stokeslet distributed along the fiber,

a set of image singularities which Blake & Chwang (1974) demonstrated will satisfy the no-slip boundary condition. The high aspect ratio allows expansion in terms of $\epsilon = \frac{1}{\ln 2\kappa}$, which is the small parameter, with $\kappa = l/a$ being the aspect ratio. We retain terms of $O(\epsilon)$ and $O(\epsilon^2)$ in this study.

While a sphere makes contact with a wall at only one separation $h^* = a$ and has zero lift velocity owing to lubrication forces at this separation, a fiber can contact the wall for $a < h^* < l$ and we will see that its lift velocity is non-zero in this range. As first observed experimentally by Stover & Cohen (1990), the edge of a fiber in Stokes flow with $a < h^* < l$ makes a solid-body contact with the wall. The resulting contact force pushes the fiber away from the wall and shifts its orientation toward smaller C, corresponding to migration away from the flow-gradient plane, in a dynamic motion the authors referred to as pole vaulting. We will show that the coupling of pole vaulting with the fluid-inertia-induced orientational changes predicted by Subramanian & Koch (2005) drives an evolution of the fiber trajectory that tends to move it away from the wall. This drift away from the wall is analytically evaluated and represents the lift velocity experienced by the fiber in this case.

In the following sections we derive the lift velocity for a slender, neutrally buoyant, cylindrical fiber to $O(\mathrm{Re})$. In §2, we use the generalized reciprocal theorem, slender-body theory and hydrodynamic wall images to determine the lift for a fiber not touching the wall, i.e $l < h^* \ll L_0$. In §3, the case of a fiber colliding with the wall is considered. Finally, in §4, we will summarise our findings, discuss the variation of the hydrodynamic lift velocity over all distances from the wall, and consider the way this result affects the sample application of cross-flow filtration.

2. Lift velocity of a fiber in the absence of wall contact

When a fiber in wall-bounded shear flow does not make contact with the wall, the asymmetric fluid stress distribution on it accounts for the hydrodynamic drift. This stress distribution can be obtained by solving the Navier-Stokes equation:

$$\nabla \cdot \boldsymbol{\sigma} = \mathrm{Re}\left[\frac{\partial \mathbf{u}}{\partial t} + \mathbf{u} \cdot \nabla \mathbf{u}\right] \qquad \nabla \cdot \mathbf{u} = 0 \tag{2.1}$$

where $\mathbf{u}$ is the fluid velocity $\boldsymbol{\sigma} = -p\mathbf{I} + 2\mathbf{e}$ is the stress, p is the pressure, and $\mathbf{e} = \frac{1}{2}\left[\nabla \mathbf{u} + \nabla \mathbf{u}^\top\right]$ is the strain rate. Here, lengths, velocities and stresses are non-dimensionalized by l,$\dot{\gamma} l$, and $\mu\dot{\gamma}$ respectively. The dimensional variables will be expressed with $*$ and their non-dimensionalised counterparts without. The imposed shear flow is $\mathbf{u}^\infty = r_2\,\mathbf{e}_1$ where we have adopted a Cartesian coordinate system with r_2 being the distance from the wall, r_1 a coordinate in the flow direction, $\mathbf{e_1}$ is a unit vector in the 1-direction, and r_3 the coordinate in the vorticity direction of the imposed flow. The fiber experiences no net force $\mathbf{F} = \int dA\,\mathbf{n} \cdot \boldsymbol{\sigma} = 0$ and no net torque $\mathbf{L} = \int dA\,\mathbf{r} \times (\mathbf{n} \cdot \boldsymbol{\sigma}) = 0$, with $\mathbf{n}$ being the outward normal from the area A into the fluid volume V, and the fluid velocity is zero on the wall. Stokes flow reversibility implies that a fiber should not experience any net drift perpendicular to the wall at zero Reynolds number. Consistent with this expectation Yang & Leal (1984) computed a time oscillatory fiber translation in the 2-direction with no net drift as the fibers rotated in a periodic motion that approximated Jeffery orbits (Jeffery 1922) . A net drift away from the wall is expected at finite Re along with the persistence of this oscillatory behaviour.

To obtain the lift velocity of the fiber at small Reynolds number in the case where the fiber lies within the viscous dominated inner region near the wall, $h^* \ll L_O$, we can expand the fluid velocity, pressure and fiber velocity in regular perturbation expansions in

the small parameter Re of the form $\mathbf{u} = \mathbf{u^0} + \mathrm{Re}\ \mathbf{u^1}$, $p = p^0 + \mathrm{Re}\ \mathrm{p}^1$, and $\mathbf{v} = \mathbf{v^0} + \mathrm{Re}\ \mathbf{v^1}$ respectively. The lift velocity can then be obtained by averaging $\mathrm{Re}\ \mathbf{v^1}$ over the Jeffery period of rotation of the fiber. The derivation of the perturbed fluid velocity $\mathbf{u^1}$ would be difficult. However, we can use a generalized reciprocal theorem to express the fiber velocity $\mathbf{v^1}$ in terms of a volume integral involving the Stokes flow field $\mathbf{u}^0$ for the shear flow problem and a comparison flow field $\mathbf{u}'$ driven by a fiber translating in the 2-direction. In the following discussion, we first present the generalized reciprocal theorem. Next the Stokes flow field and comparison field is expressed using slender-body theory and hydrodynamic images with the wall. After that we discuss the averaging of the lift velocity over the Jeffery period of rotation and other details of the lift velocity calculation.

The generalized reciprocal theorem for a problem with weak fluid inertia (see Lovalenti & Brady 1993) can be obtained by considering the volume integral

$$\int \nabla \cdot [\boldsymbol{\sigma}^1 \cdot \boldsymbol{u}' - \boldsymbol{\sigma}' \cdot \boldsymbol{u}^1] dV \tag{2.2}$$

where $\mathbf{u}'$ and $\boldsymbol{\sigma}'$ are the fluid velocity and stress field for a Stokes flow comparison problem that satisfies

$$\nabla \cdot \boldsymbol{\sigma}' = 0$$

and

$$\nabla \cdot \boldsymbol{u}' = 0$$

along with boundary conditions $\mathbf{n} \cdot \boldsymbol{\sigma}' = \frac{1}{A_f}\, \mathbf{e_2}$ on the fiber and $\mathbf{u}' = \mathbf{0}$ on the walls and at large distances from the fiber. Here A_f is the surface area of the fiber.

Using the divergence theorem, one can obtain

$$\begin{aligned}\int \nabla \cdot [\boldsymbol{\sigma}^1 \cdot \boldsymbol{u}' - \boldsymbol{\sigma}' \cdot \boldsymbol{u}^1] dV = &\int_{\text{fiber}} dA\, \mathbf{n} \cdot [\boldsymbol{\sigma}' \cdot \boldsymbol{u}^1 - \boldsymbol{\sigma}^1 \cdot \boldsymbol{u}'] + \int_{\text{wall}} dA\, \mathbf{n} \cdot [\boldsymbol{\sigma}' \cdot \boldsymbol{u}^1 - \boldsymbol{\sigma}^1 \cdot \boldsymbol{u}'] \\ &+ \int_{\infty} dA\, \mathbf{n} \cdot [\boldsymbol{\sigma}' \cdot \boldsymbol{u}^1 - \boldsymbol{\sigma}^1 \cdot \boldsymbol{u}'] \end{aligned} \tag{2.3}$$

The no-slip boundary condition implies that the integral on the wall vanishes. The fluid velocity disturbance due to the fiber decays as $\frac{1}{r^2}$ in both the shear and comparison problem so the integral on the bounding surface vanishes as its distance goes to infinity. Finally, the rigid-body motion, no-force and no-torque conditions on the fiber in shear flow along with the specified force density on the fiber ($\int dA\, \mathbf{n} \cdot \boldsymbol{\sigma}' = \mathbf{e}_2$) in the comparison problem simplify the surface integral on the fiber to yield

$$\int \nabla \cdot [\boldsymbol{\sigma}^1 \cdot \boldsymbol{u}' - \boldsymbol{\sigma}' \cdot \boldsymbol{u}^1] dV = \mathbf{v^1} \cdot \mathbf{e_2} \tag{2.4}$$

The equations of motion for the shear flow and comparison problem yield

$$\int \nabla \cdot [\boldsymbol{\sigma}^1 \cdot \boldsymbol{u}' - \boldsymbol{\sigma}' \cdot \boldsymbol{u}^1] dV = \mathrm{Re} \int \left[\frac{\partial \mathbf{u}^0}{\partial t} + \mathbf{u}^0 \cdot \nabla \mathbf{u}^0 \right] \cdot \boldsymbol{u}' dV \tag{2.5}$$

Combining (2.4) and (2.5), we obtain an expression for the inertia-induced translational velocity of the fiber perpendicular to the wall in terms of the Stokes flow shear and comparison fluid velocity fields

$$\mathrm{Re} \mathbf{v}^1 \cdot \mathbf{e}_2 = \mathrm{Re} \int \left[\frac{\partial \mathbf{u}^0}{\partial t} + \mathbf{u}^0 \cdot \nabla \mathbf{u}^0 \right] \cdot \boldsymbol{u}' dV \tag{2.6}$$

The Stokes flow field $\mathbf{u}^0$ consists of the imposed flow ($\mathbf{u}^\infty$) and the disturbance field

($\mathbf{u}^{\mathrm{D}}$), created by the presence of the fiber and the no-slip wall. This disturbance velocity field can be captured by a collection of singularities along with the driving force behind it. The driving force experienced by the fiber in quiescent flow is qualitatively and quantitatively different from when it is placed in a shear flow. However, the system of singularities remains the same in both cases.

A thin fiber in low Re flow can effectively be replaced by a collection of Stokeslet, the fundamental singularity in a Stokes flow. A Stokeslet near a no-slip wall was studied by Blake & Chwang (1974). They found that a no-slip wall at $(r_1, r_2 = 0, r_3)$, in the presence of a Stokeslet placed at $\mathbf{r}^f$, can be replaced by another Stokeslet as well as a force dipole and a potential dipole placed at $\mathbf{r}^{im} = (r_1^f, -r_2^f, r_3^f)$. These singularities are mathematically represented by Green's function. The overall non-dimensional Green's function of the fiber and no-slip wall system causing disturbance to the fluid velocity at $\mathbf{r}$ is given by,

$$\mathbf{G}(\mathbf{r}, s) = \mathbf{G}^{\mathrm{S}}(\overline{\mathbf{r}}) - \mathbf{G}^{\mathrm{S}}(\overline{\mathbf{r}}^{im}) - 2(r_2^f)\mathbf{G}^{\mathrm{FD}}(\overline{\mathbf{r}}^{im}) + 2(r_2^f)^2\mathbf{G}^{\mathrm{PD}}(\overline{\mathbf{r}}^{im}) \tag{2.7}$$

Here, $\overline{\mathbf{r}} = \mathbf{r} - \mathbf{r}^f$ and $\overline{\mathbf{r}}^{im} = \mathbf{r}^{im} - \mathbf{r}^f$. Any point on the fiber can be expressed as $\mathbf{r}^f = \mathbf{r}^c + \mathbf{p}\ s$. $\mathbf{r}^c$ is the centre of the fiber, $\mathbf{p}$ is the unit vector along the axis of the fiber and s represents the co-ordinate along the fiber length. s ranges from -1 to 1 and thus spans all of the thin fiber's geometry. $\mathbf{G}^{\mathrm{S}}$ is the Stokeslet, $\mathbf{G}^{\mathrm{FD}}$ is the force dipole. and $\mathbf{G}^{\mathrm{PD}}$ is the potential dipole. The individual functions, non-dimensionalised by μ, are given as,

$$G_{ij}^{S}(\mathbf{r}) = \frac{1}{8\pi\ r}\left[\delta_{ij} + \frac{r_i r_j}{r^2}\right] \tag{2.8}$$

$$G_{ij}^{FD}(\mathbf{r}) = \frac{1}{8\pi}\left[r_2 G_{ij}^{PD}(\mathbf{r}) \pm \frac{\delta_{j2} r_i - \delta_{i2} r_j}{r^3}\right] \tag{2.9}$$

$$G_{ij}^{PD}(\mathbf{r}) = \pm\frac{1}{8\pi\ r^3}\left[\delta_{ij} - 3\frac{r_i r_j}{r^2}\right] \tag{2.10}$$

In equations (2.9) and (2.10) there is a plus sign for j = 1 and 3 and a minus sign for j = 2. Thus it is possible to obtain $\mathbf{u}^{\mathrm{D}}$ at any fluid location $\mathbf{r}$ through an integral in s, spanning the whole length of the fiber as,

$$u_i^{\mathrm{D}}(\mathbf{r}) = \int_{-1}^{1} ds\, f_j(s)\, G_{ji}(\mathbf{r}, s) \tag{2.11}$$

where $\mathbf{f}(s)$ is the force distribution on the fiber.

To evaluate $\mathbf{u}^{\mathrm{D}}$ the force per unit length $\mathbf{f}(s)$ needs to be determined. From slender-body theory (see Batchelor 1970) the governing equation for $\mathbf{f}(s)$ is given as,

$$\begin{aligned} v_i^0 + \epsilon_{ijk}\Omega_j\, p_k s = w_i(\mathbf{r}^c + \mathbf{p}\, s) + \frac{f_j}{4\pi}[\delta_{ij} + p_i p_j][\ln 2\kappa + \ln[\frac{[1-s^2]^{\frac{1}{2}}}{a(s)}]] \\ + \frac{f_j}{8\pi}[\delta_{ij} - 3p_i p_j] + \frac{f_j}{8\pi}[\delta_{ij} + p_i p_j]\int_{-1}^{1} \frac{f_j(s') - f_j(s)}{\mid s - s' \mid}\, ds' \end{aligned} \tag{2.12}$$

where $\mathbf{v}^0$ and $\boldsymbol{\Omega}$ are the fiber centre of mass translational and rotational velocities at zero Re, $a(s)$ is the radius of the fiber at any given location on the fiber normalized with the characteristic radius. $a(s) = 1$ for a cylindrical fiber. $\kappa = \frac{l}{a}$ is the aspect ratio. $\mathbf{w}$ is the far field velocity consisting of the imposed shear flow and image velocity. In solving

equation (2.12) we assume the fiber has a large aspect ratio and expand in terms of the small parameter $\epsilon = \frac{1}{\ln 2\kappa}$. This leads to a perturbation in ϵ for $\mathbf{f}$ as well as $\mathbf{v}^0, \mathbf{w}, \mathbf{u}^{\mathrm{D}}$ and $\dot{\mathbf{p}}$. These can be expressed as,

$$\begin{aligned}
\mathbf{f} &= \epsilon \mathbf{f}_1 + \epsilon^2 \mathbf{f}_2 + ... \\
\dot{\mathbf{p}} &= \dot{\mathbf{p}}_0 + \epsilon \dot{\mathbf{p}}_1 + ... \\
\mathbf{v}^0 &= \mathbf{v}_0^0 + \epsilon \mathbf{v}_1^0 + ... \\
\mathbf{w} &= \mathbf{w_0} + \epsilon \mathbf{w_1} + ... \\
\mathbf{u}^{\mathrm{D}} &= \epsilon \mathbf{u}_1^{\mathrm{D}} + \epsilon^2 \mathbf{u}_2^{\mathrm{D}} + ...
\end{aligned} \tag{2.13}$$

The subscripts here denote the order of the term with respect to the expansion in ϵ. In this study we compute the lift velocity to $O(\epsilon^2)$ by retaining the terms indicated in equation (2.13) for the force per unit length, fiber rotation and translation rate, far field velocity and fluid velocity disturbance.

To obtain $\mathbf{u_1^{\mathrm{D}}}$, the leading order disturbance velocity field in the ϵ expansion, we evaluate $\mathbf{f_1}$. The force distribution on the fiber at $O(\epsilon)$ is given as,

$$\frac{1}{4\pi} f_{1,i}[\delta_{ij} + p_i p_j] = v_i^0 + \epsilon_{ijk}\Omega_j p_k s - w_{0,i}(\mathbf{r}^c + \mathbf{p}\, s) \tag{2.14}$$

At leading order in ϵ, the far field velocity $\mathbf{w_0}$ is the imposed shear flow $\mathbf{u}^\infty$. In a simple shear flow the dynamics of the fiber motion at finite Re was studied by Subramanian & Koch (2005). They showed that inertia forces the fiber towards motion in the flow-gradient plane. This constraint simplifies equation (2.14) to,

$$\mathbf{f}_1 = 4\pi\, \mathbf{p}\, s \cos\phi \sin\phi \tag{2.15}$$

Here ϕ is the dihedral angle between the flow-vorticity and the fiber-vorticity planes.

To obtain $\mathbf{u_2^{\mathrm{D}}}$ we obtain the force distribution at $O(\epsilon^2)$ as,

$$f_{2,j} = \pi p_i \sin 2\phi[2s\ln[1-s^2] - 3s] - 4\pi[\delta_{ij} - \frac{p_i p_j}{2}]\, w_{1,i}(\mathbf{r}^c + \mathbf{p}\, s) \tag{2.16}$$

To evaluate $\mathbf{w}_1$ we use the disturbance velocity result from equation (2.11) and evaluate only the image component. This is given as,

$$\mathbf{w}_1(\mathbf{r}) = \int_{-1}^{1} ds\, f_{1,j}(s)\, G_{ji}^{\mathrm{I}}(\mathbf{r}, s) \tag{2.17}$$

Here $G_{ji}^{\mathrm{I}}(\mathbf{r}, s)$ is due to the image system that captures wall reflection. This is given as,

$$\mathbf{G}^{\mathrm{I}}(\mathbf{r}, s) = -\mathbf{G}^{\mathrm{S}}(\bar{\mathbf{r}}^{im}) - 2(r_2^f)\mathbf{G}^{\mathrm{FD}}(\bar{\mathbf{r}}^{im}) + 2(r_2^f)^2\mathbf{G}^{\mathrm{PD}}(\bar{\mathbf{r}}^{im}) \tag{2.18}$$

With a complete description of $\mathbf{G}(\mathbf{r}, s)$ and $\mathbf{f}(\mathbf{s})$ known at the first two orders in ϵ, equation (2.11) can be evaluated to find $\mathbf{u}^{\mathrm{D}}$ and by extension $\mathbf{u^0}$. To evaluate equation (2.6) and obtain lift velocity information on $\boldsymbol{u'}$ is also needed. In the quiescent comparison flow the disturbance velocity field is calculated using equation (2.11) with a specified force distribution $\int \mathbf{f'}(s)\, ds = \int dA\mathbf{n} \cdot \boldsymbol{\sigma'} = \mathbf{e}_2$.

The fiber rotates in a shear flow and samples all possible orientations in the flow-gradient plane. Orientation plays an important role in determining $\mathbf{f}(s)$, as evident by the strong dependence on ϕ in equation (2.15) and (2.16). Hence it is desirable to obtain a time-averaged lift velocity by averaging equation (2.6) over a characteristic time period, that will later be shown to be the Jeffery period, T as,

$$v_l = \frac{\mathrm{Re}}{T} \int_0^T dt\, \mathbf{v}^1 \cdot \mathbf{e}_2 \tag{2.19}$$

Thus we get,

$$v_l = \frac{\mathrm{Re}}{T}\int_0^T dt \int dV \left[\frac{\partial \mathbf{u}^0}{\partial t} + \mathbf{u}^0 \cdot \nabla \mathbf{u}^0\right] \cdot \boldsymbol{u}' \tag{2.20}$$

A regular perturbation in ϵ similar to those expressed in equation (2.13) can be extended to this time-averaged lift velocity and is given as,

$$v_l = \epsilon \;\; v_{l1} + \epsilon^2 \;\; v_{l2} + ... \tag{2.21}$$

It is evident that $v_{l0} = 0$ due to the nature of the force distribution. We will evaluate the first two non-zero terms v_{l1} and v_{l2} in this study.

Yang & Leal (1984) studied the temporal evolution of fibers in Stokes flow and found that, at zero Re, they undergo periodic flipping motion. This periodic motion is expected to persist at small, but finite, Re. At zero Re Jeffery (1922) studied the periodic orbits of ellipsoidal particles in an unbounded simple shear flow. Jeffery's calculation properly captures the flipping motion of fibers near a wall, as shown in experimental studies carried out by Stover & Cohen (1990) and Moses *et al.* (2001). In this study we will assume that these periodic orbits (commonly referred to as Jeffery Orbits) describe the temporal dynamics of the fiber at finite Re near a wall and the Jeffrey time period is the characteristic time period T.

In any Jeffrey orbit the evolution of ϕ can be given as,

$$\cot\phi = \kappa \;\; \cot\left[\frac{2\pi t}{T}\right] + \cot\phi_0 \tag{2.22}$$

where ϕ_0 is the angle at time 0. The time period T for one revolution is given as,

$$T = 2\pi\left[\kappa + \frac{1}{\kappa}\right] \tag{2.23}$$

In calculating the lift velocity through equation (2.20), the average over time is transformed to one over angle ϕ using equation (2.22). Owing to the quasi-steady nature of Stokes flow the partial derivative of the fluid velocity can be related to the time variation of the fiber orientation and centre of mass position,

$$\frac{\partial \mathbf{u}^0}{\partial t} = \frac{\partial \mathbf{u}^0}{\partial \phi}\frac{\partial \phi}{\partial t} + \frac{\partial \mathbf{r}^c}{\partial t} \cdot \nabla \mathbf{u}^0 \tag{2.24}$$

While computing the $O(\epsilon)$ lift velocity, the time dependence of $\mathbf{r}^c$ can be removed by adopting a reference frame translating with the $O(1)$ particle translational velocity and $\partial\phi/\partial t$ can be evaluated using the Jeffery orientation (2.22). At $O(\epsilon^2)$ there are additional contributions to the time derivatives of the fiber orientation and position caused by the $O(\epsilon)$ wall reflection fluid velocity disturbance. These are given as,

$$\begin{aligned} \dot{p}_{1,i} &= \frac{3}{2}\int_{-1}^{1} ds\,[\delta_{ij} - p_{0,i}p_{0,j}]w_{1,j}(\mathbf{r}^c + \mathbf{p}\,s)s \\ \mathbf{v}_1^0 &= \frac{1}{2}\int_{-1}^{1} ds\,\mathbf{w}_1(\mathbf{r}^c + \mathbf{p}\;\; s) \end{aligned} \tag{2.25}$$

$\mathbf{w}_1$ is given in equation (2.17).

The lift velocity calculation involves nested integrals spanning a large domain. The spatial co-ordinate r_i spans $-\infty$ to ∞ when $i = 1, 3$ and 0 to ∞ for $i = 2$, thus capturing all of the fluid volume. Based on symmetry, the angular integration in ϕ from 0 to 2π can be related to 4 times the integral from 0 to $\pi/2$. The disturbance velocity field driving the

lift velocity involves an integral over s, thus capturing the net effect of the singularities of the fiber and it's images. The higher order (in ϵ) force distribution as well as unsteadiness (see equation (2.25)) depend on the image velocity, which in turn requires integration over s for the image singularities. All of these nested integrals are numerically evaluated using an adaptive quadrature scheme. For this purpose a combination of the 'integral' and 'integral2' routines available in MATLAB are used.

The dimensional lift velocity (v_l^*) of a fiber will be proportional to the characteristic shear velocity $\dot{\gamma}l$ based on the chosen non-dimensionalization. However it is modified by three factors: fluid inertia, flipping motion in a Jeffery orbit and the thinness of the fiber. In the absence of fluid inertia, i.e Stokes flow, there is no net migration. At small but finite Reynolds number, the lift velocity is proportional to Re. In a Jeffery orbit the time period is $O(\kappa)$ whereas the flipping motion, during which significant migration away from the wall occurs, takes place over $O(1)$ time. Thus a factor of κ^{-1} appears in the time-averaged lift velocity. Finally, the disturbance velocity field, that drives the migration away from the wall, is shaped by the geometry of the fiber. For a high aspect ratio fiber this is characterised by ϵ. So, the scaling of the lift velocity can be given as $\rho\dot{\gamma}^2 l^2 a/(\mu \ln\left[\frac{2l}{a}\right])$ when not making contact with the wall.

In contrast to a fiber, the hydrodynamic lift on a sphere, while also being a finite Re effect, has none of the complexities associated with orientation and aspect ratio. So, the dimensional lift velocity of a sphere scales as, $\rho\dot{\gamma}^2 a^3/\mu$, where a is the characteristic length of the sphere which is it's radius. Figure 1 gives the variation of the lift velocity of a sphere with distance from the wall in the inner region. The lift velocity is scaled as $\rho\dot{\gamma}^2 a^3/\mu$ in this plot. This result is obtained using the lift force derived by Cherukat & McLaughlin (1994), and using the special case of no force along the streamline from their analysis, along with the appropriate Stokes resistance function(see Brenner 1961; Cox & Brenner 1967). The lift force does not necessarily go to zero as the sphere approaches the wall but the Stokes resistance function, due to lubrication effects, always diverges leading to a decay of lift velocity on a sphere to zero. Conversely the resistance decays away from the wall and so the lift velocity approaches a constant at separations that are large but still lie within the inner region.

Figure 2 presents the computed lift velocity for the fiber at $O(\epsilon\ \mathrm{Re})$. The lift velocity presented is scaled as $\rho\dot{\gamma}^2 l^2 a/(\mu \ln\left[\frac{2l}{a}\right])$ and given as a function of the non-dimensional distance of the centre of the fiber from the wall. When the fiber approaches the wall its lift velocity, unlike a sphere, does not tend to zero. This can be attributed to the finite Stokes resistance for the sharp edges of the fiber as pointed out by Harlen *et al.* (1999). These sharp ends can make contact with the wall in finite time. Additionally, the fiber end only contacts the wall at one instant in time during the fiber's periodic motion when $h^* = l$. As the distance from the wall increases the Stokes resistance experienced decreases and the lift velocity increases monotonically. At large distances from the wall, but still in the inner region, the lift velocity asymptotes at leading order to a value of $0.0303\rho\dot{\gamma}^2 l^2 a/(\mu \ln\left[\frac{2l}{a}\right])$. Qualitatively, at $O(\epsilon)$, the lift velocity captures the breaking of the stress symmetry that leads to a net migration due to a simple interaction of the imposed shear flow with a thin geometry.

Figure 3 shows the O (Re) fiber lift velocity at based on the first two terms of the slender body theory expansion at various κ plotted as a function of the non-dimensional distance from the wall. Despite scaling the lift velocity with the leading order scaling of $\rho\dot{\gamma}^2 l^2 a/(\mu \ln\left[\frac{2l}{a}\right])$, there remains a significant dependence on the aspect ratio with the lift velocity reaching significantly higher values at smaller aspect ratio. Even at an aspect ratio as high as 10^4, the asymptotic value of the total lift velocity is about 50% larger than the $O(\epsilon)$ lift velocity. This indicates that a significant contribution to the

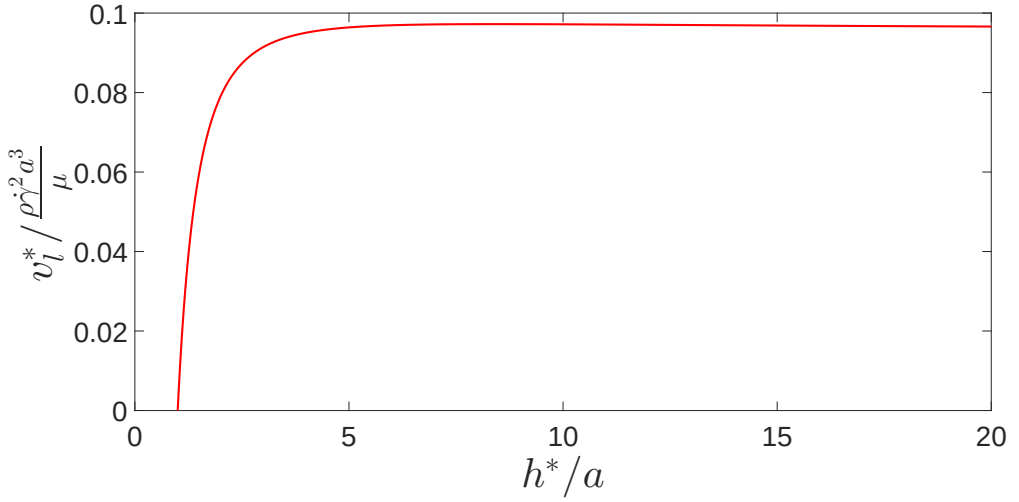

FIGURE 1. Lift velocity for a sphere as a function of distance from the wall in the inner region. h^* represents the dimensional distance of the sphere of radius a from the wall. The lift velocity is obtained using the lift force calculation of Cherukat & McLaughlin (1994) in conjunction with Stokes resistance functions (see Brenner 1961; Cox & Brenner 1967)

.

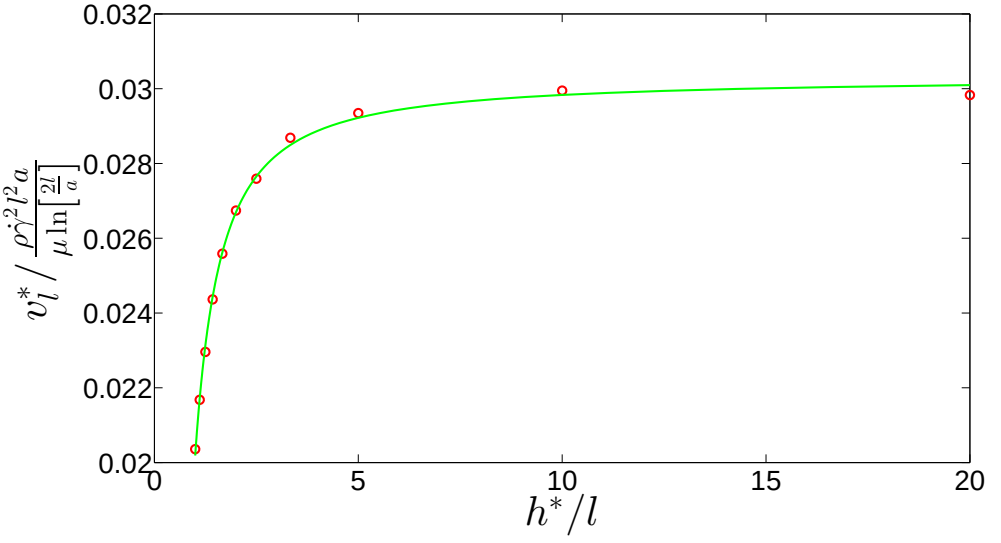

FIGURE 2. Variation of the $O(\epsilon \mathrm{Re})$ fiber lift velocity as a function of distance from the wall. Circles show the evaluated data and the line shows the fit given by $v_{l1} = -0.0057/h^2 - 0.0044/h + 0.0303$.

lift velocity comes from the $O(\epsilon^2)$ term. This higher order term includes a number of qualitative features not present at $O(\epsilon)$ including the influence of the wall reflection, the oscillatory translation of the fiber perpendicular to the wall, and the effects of the precise variation of the fiber thickness as captured by the $\ln[(1-s^2)^{\frac{1}{2}}/a(s)]$ term in equation (2.12). At $O(\epsilon^3)$ and higher orders, no qualitatively new mechanisms come into play, so we have restricted the analysis to the first two terms in the expansion in ϵ.

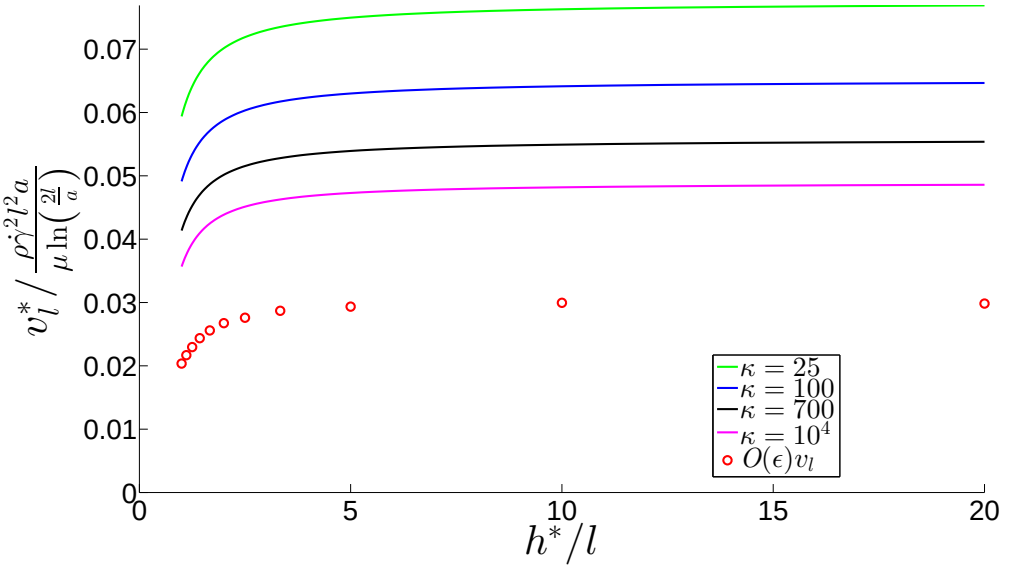

FIGURE 3. Variation of the O (Re) lift velocity calculated based on the first two terms of the slender body theory expansion for a fiber and expressed as a function of distance from the wall at various aspect ratios. The aspect ratio of the curves going from highest to lowest asymptote values are 25,100,700,10^4. Circles represent the lift velocity at $O(\epsilon)$

3. Lift velocity of a fiber experiencing wall contacts

When $h < 1$ the dominant contribution to the lift velocity of a fiber in wall-bounded shear flow of small but finite inertia comes from the normal force due to solid-body contact coupled with inertial rotation. For $h < 1$ the orbit in the flow-gradient plane preferred based on inertial rotation is no longer accessible. Thus, the inertial torque driving the fiber toward the flow-gradient plane and the wall contact force compete to influence the fiber orientation. In this section, we will analyse the coupled action of these two mechanism. First we will track the trajectory of the fiber for $h < 1$. Then we will develop an analytical model for the lift velocity in the $h < 1$ regime by assuming the fiber follows a quasi-steady Jeffery orbit that just grazes a frictionless wall. This model is then validated by comparison with the numerically computed trajectory.

A fiber in a simple shear flow adjacent to a wall is pushed away from it by the wall contact force. In addition, any fiber with an orientation out of the flow-gradient plane is pushed further out of the plane. This effect was experimentally observed by Stover & Cohen (1990) and they referred to it as pole vaulting. A number of studies (see Ku & Lin 2009; Jayageeth *et al.* 2009; Scheuer *et al.* 2016; Nagel *et al.* 2018) have built on Stover and Cohen's work and analysed the trajectory of wall-bounded fibers in Stokes flow. At finite Re many studies have looked at dynamics of spheroids in an unbounded flow (see Khayat & Cox 1989; Subramanian & Koch 2005; Einarsson *et al.* 2015*a*,*b*; Dabade *et al.* 2016; Marath & Subramanian 2017), but none have considered the effects of wall contact. So, in this study, we will couple the displacement and orientation perturbation due to pole vaulting with the inertial orientation drift predicted by Subramanian & Koch (2005) to numerically compute the fiber trajectory. This fiber trajectory calculation does not include the direct effects of inertial translation discussed in §2. It will be shown a posteriori, through the analytical model of the wall contact lift velocity and it's scaling, that inertial translation is weaker by a factor of the aspect ratio compared to motion driven by inertial rotation coupled with wall contact.

Subramanian & Koch (2005) showed that a fiber orientation at finite Re tends to move towards the flow-gradient plane. They showed this by first computing the finite Re correction to the equations governing the orientation the fiber. $\mathbf{p}$ can be fully described through θ, the polar angle between the fiber axis and the vorticity direction, and ϕ, the dihedral angle between the flow-vorticity and the fiber-vorticity planes. These evolve in time as,

$$\dot{\theta}_{\hat{I}} = \sin\theta\cos\theta\sin\phi\cos\phi\left[1 + \frac{14\epsilon'\mathrm{Re}}{15}\sin^2\theta\sin\phi\cos\phi\right] \tag{3.1}$$

$$\dot{\phi}_{\hat{I}} = \frac{-1}{\kappa^2+1}[\kappa^2\sin^2\phi + \cos^2\phi] \\ -\epsilon'\mathrm{Re}\sin\theta\sin\phi\cos\phi\left[\frac{2}{3}\sin\theta\sin^2\phi - \frac{4}{15}\sin\theta\cos^2\phi\right] \tag{3.2}$$

The subscript $\hat{I}$ indicates that this rotation includes effects of fluid inertia and excludes the influence of the wall. It should be noted that a slightly different definition of the small parameter was used in their study. It is given as $\epsilon' = \frac{1}{\ln\kappa}$. In these equations the $\sin\theta\cos\theta\sin\phi\cos\phi$ term is the original Jeffery result for θ evolution without inertia. The equivalent inertia-less component for ϕ is $\frac{-1}{\kappa^2+1}[\kappa^2\sin^2\phi + \cos^2\phi]$. The inclusion of the inertial correction to these Jeffery equations leads to $\theta \to \pi/2$. This corresponds to drift of the fiber motion towards the flow-gradient plane.

At zero Re each of the unique Jeffery orbits is associated with an orbit constant given as,

$$\mathrm{C} = \frac{\tan\theta\left[\kappa^2\sin^2\phi + \cos^2\phi\right]^{\frac{1}{2}}}{\kappa} \tag{3.3}$$

that is invariant during its evolution and ranges from 0 (flow-vorticity plane) to ∞ (flow-gradient plane). Small, but finite, inertia acts to shift the fiber from a lower orbit constant to higher one, eventually spiralling to $C = \infty$. On the other hand, pole vaulting shifts the fiber to a lower orbit constant (see Stover & Cohen 1990).

The finite inertia correction to the Jeffery orbit was computed in an unbounded shear flow, but it can be used to describe the leading order rotation in the $0 < h < 1$ regime. The effects of the hydrodynamic wall reflections on the orientational drift are $O(\epsilon')$ smaller than the leading order result captured by (3.1) and (3.2). In addition, the fiber spends most of the time without direct contact with the wall so that the effects of wall contact and fluid inertia on orientational drift can be superimposed.

When $0 < h < 1$, the fiber can make solid-body contact with the wall during its flipping motion. A numerical study by Harlen *et al.* (1999) illustrates the idea of using a solid-body wall-fiber contact when the sharp edges of a high aspect ratio fiber contact a surface (that of a falling ball in their study). Harlen *et al.* (1999) argued that wall contact can occur due to the sharp edge of a fiber reducing the lubrication resistance. Even for smooth edged fibers, it was argued that the driving force pushing the fiber toward the wall scales with the fiber length while the lubrication force scales with the much smaller radius, so that lubrication breaks down and wall contact is achieved.

During the short period when the fiber makes solid-body contact with the wall a constraint that the fiber end touches the wall is applicable, i.e., $r_2^{\mathrm{end}} = 0$ with the position of the end of the fiber given as $\mathbf{r}^{\mathrm{end}} = \mathbf{r}^{\mathbf{c}} + \mathbf{p}$, where $\mathbf{r}^{\mathbf{c}}$ is the centre of the fiber and $\mathbf{p}$ is the unit vector along the axis of the fiber. During contact, equations (3.1) and (3.2) are no longer applicable and instead we derive expressions for the contact-

influenced translation and rotation of the fiber in Stokes flow. The wall contact normal force for a frictionless surface can be expressed as $\mathbf{F}_{\mathrm{N}} = F_{\mathrm{N}}\mathbf{e}_2$. Subscript N, in this section, denotes that the effect arises due to wall contact. This force is determined by the no-penetration condition as long as F_{N} is positive. The force goes to zero and the no-penetration condition is no longer needed if the solution for F_{N} changes sign. Thus it can be seen that during the short period of wall contact h shows temporal evolution. The temporal dynamics of θ and ϕ evolution are also altered. To derive this modified dynamics we consider the slender-body equation and derive the new force per unit length $\mathbf{f}_{\mathrm{N}}$ in the presence of wall contact. The contact-induced translational $\mathbf{v}_{\mathrm{N}}^{\mathbf{0}}$ and rotational $\boldsymbol{\Omega}_{\mathrm{N}}$ velocities of the fiber to leading order in ϵ' are given by,

$$\frac{1}{4\pi\epsilon'} f_{\mathrm{N,j}}[\delta_{ij} + p_i p_j] = v^0_{\mathrm{N,i}} + \epsilon_{ijk}\Omega_{\mathrm{N,j}} p_k s - w_i(s) \tag{3.4}$$

Here, $\mathbf{w}$, the far-field velocity, corresponds to only the imposed shear flow since the image disturbance velocity is higher order in ϵ'. The net hydrodynamic force of the fiber on the fluid due to the contact balances the contact force $\mathbf{F}_{\mathrm{N}}$, so that

$$\int_{-1}^{1} \mathbf{f}_{\mathrm{N}}\, ds = \mathbf{F}_{\mathrm{N}} \tag{3.5}$$

The torque balance is given as,

$$\int_{-1}^{1} s\mathbf{p} \times \mathbf{f}_{\mathrm{N}}\, \mathbf{ds} = \mathbf{p} \times \mathbf{F}_{\mathrm{N}} \tag{3.6}$$

Solving equation (3.4) in conjunction with equations (3.5) and (3.6) gives the contact-induced motion of the centre of the fiber as,

$$v^0_{\mathrm{N,i}} = \frac{F_{\mathrm{N}}}{8\pi\epsilon'}\delta_{j2}\left[\delta_{ij} + p_i p_j\right] \tag{3.7}$$

The contact-induced change of the fiber's orientation vector is given as,

$$\dot{p}_{\mathrm{N,i}} = \frac{3F_{\mathrm{N}}}{8\pi\epsilon'}\delta_{j2}\left[\delta_{ij} - p_i p_j\right] \tag{3.8}$$

The evolution of $\mathbf{p}$ due to wall contact can be expressed in terms of θ and ϕ as,

$$\begin{aligned} \dot{\theta}_{\mathrm{N}} &= F_{\mathrm{N}}\frac{3\cos\theta\sin\phi}{8\pi\epsilon'} \\ \dot{\phi}_{\mathrm{N}} &= F_{\mathrm{N}}\frac{3\cos\phi}{8\pi\epsilon'\sin\theta}. \end{aligned} \tag{3.9}$$

To complete the description of the dynamics during wall contact F_{N} needs to be determined. To obtain the normal force we will use the kinematic constraint $\dot{r}_2^{\mathrm{end}} = 0$. To obtain $\dot{r}_2^{\mathrm{end}}$ we need the full dynamics of the fiber, including the effect of both inertia and the contact force. The overall dynamics of the fiber in the $h < 1$ configuration during sold-body contact can be expressed as,

$$\begin{aligned} \mathbf{v}^0 &= \mathbf{v}^0_{\mathrm{N}} \\ \dot{\theta} &= \dot{\theta}_{\mathrm{N}} + \dot{\theta}_{\hat{f}} \\ \dot{\phi} &= \dot{\phi}_{\mathrm{N}} + \dot{\phi}_{\hat{f}} \end{aligned} \tag{3.10}$$

From this we can obtain the equations governing motion in 2-direction as well as the orientation. This is given as,

$$v^0_2 = \frac{F_{\mathrm{N}}}{8\pi\epsilon'}[1 + p_2^2]$$

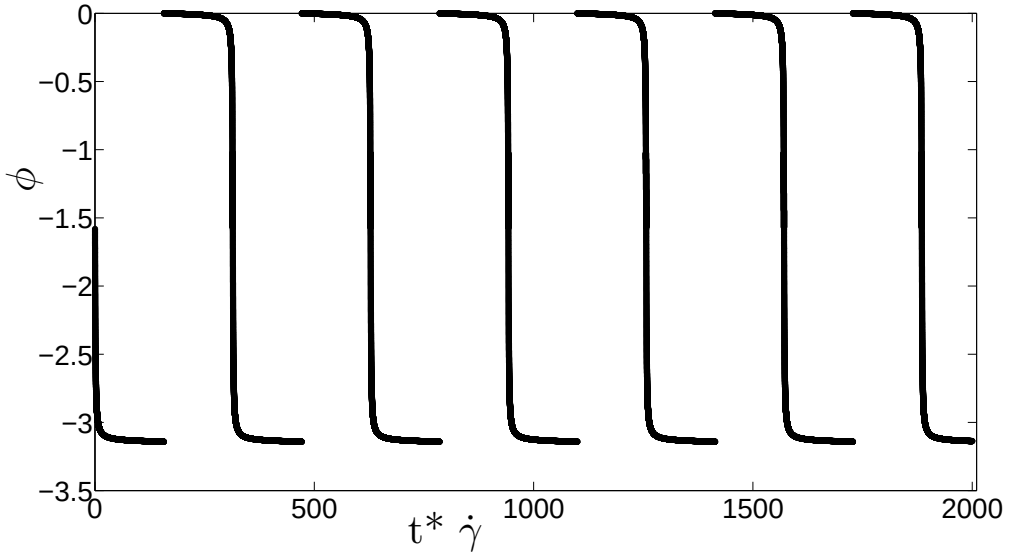

FIGURE 4. Variation of the angle ϕ (in radians) of the fiber end closest to the wall for $\kappa = 100$ and Re=10^{-3}.

$$\dot{p}_2 = \dot{p}_{\hat{I},2} + \frac{3F_{\rm N}}{8\pi\epsilon'}[1 - p_2^2] \tag{3.11}$$

The component of the fiber orientation in the 2-direction is given as $p_2 = \sin\theta \sin\phi$. The contact normal force can now be evaluated by solving $v_2^0 + \dot{p}_2 = 0$ to obtain,

$$F_{\rm N} = \frac{8\pi\epsilon' \left[-\dot{p}_{\hat{I},2}\right]}{[4 - 2p_2^2]} \tag{3.12}$$

To track the trajectory of the fiber we integrate equations (3.10) with results supplied from equation (3.1), (3.2), (3.8), (3.9) and (3.12). The choice of time steps is important in the trajectory evolution as both flipping and wall contact are very short lived phenomena. The short lived flipping can be expected from equation (2.22) and evident from figures 4,5, and 6 that show the evolution of ϕ, θ and h. Based on equation (2.22) flipping can be properly captured by choosing a time step of about $T/2\pi\kappa$. The wall contact is even shorter as it results from the small inertial perturbation of the fiber orbit between two successive wall contacts. An adaptive time stepping is used to capture the wall contact.

The variation of ϕ and θ is shown in figures 4 and 5 respectively. For numerical efficiency only the ϕ associated with the half-fiber closest to the wall is tracked and so ϕ is bound between 0 and $-\pi$. The change of reference fiber arm is seen in figure 4 as a discontinuity. The fiber spends long periods of time nearly aligned with the flow-vorticity plane, with $\phi \approx 0$ or $-\pi$, and then rapidly flips and makes a wall contact. The short lived flipping and wall-contact phase corresponds, in figure 5, to the dip in θ to a minima of θ_m, away from the flow aligned state of $\theta \approx \pi/2$. By tracking changes to θ_m, which can be related to C through equation (3.3), it is possible to quantify orbital drift due to inertia and wall contacts.

Wall contact occurs during a very small fraction of the orbital motion of the fiber, but it is the sole pathway to increasing the height of the fiber. This is evident in figure 6 where h behaves like a step function with the transitions corresponding to solid-body contact with the wall. These jumps at wall contact are additive. Eventually a fiber starting at

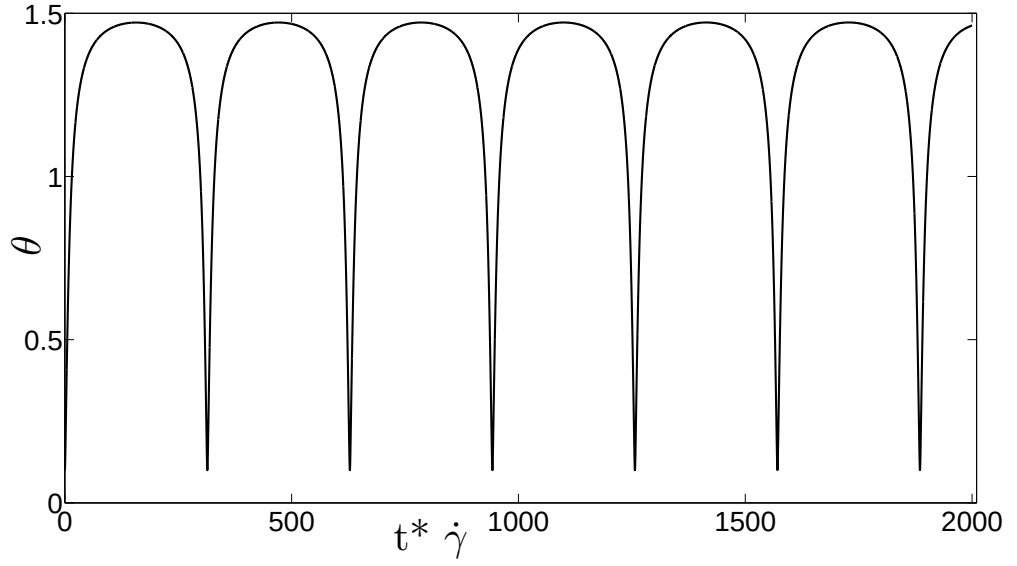

FIGURE 5. Variation of the angle θ (in radians) of a fiber with $\kappa = 100$ in a flow with Re=10^{-3}.

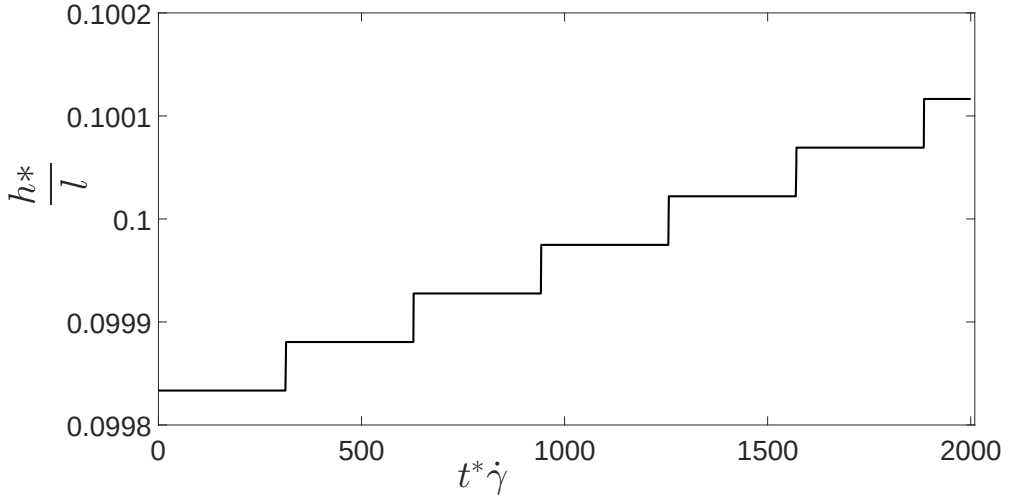

FIGURE 6. Trajectory of the fiber centre-of-mass for $\kappa = 100$ in a flow with Re=10^{-3}

any $0 < h < 1$ ends up at $h = 1$. This can be observed in figure 7 which shows the evolution of h observed over a longer duration. The upward drift of the centre of mass of the fiber can be considered its lift velocity ($v_{l,\mathrm{N}}$). To obtain this lift velocity we consider a quasi-steady orbit that, for the given value of h, just makes contact with the wall. In this configuration we will find the shift in the height of the centre of mass of a fiber and average it over the time period of the orbit to obtain the lift velocity.

In the quasi-steady orbit model, we assume that the fiber makes contact with the wall at exactly $\phi = -\pi/2$ and $\theta = \theta_m$. We evaluate the shift in height of the fiber using a kinematic constraint. This will capture the total drift of the fiber from the wall as it evolves in a sequence of quasi-steady orbits while the fiber end continues to brush the

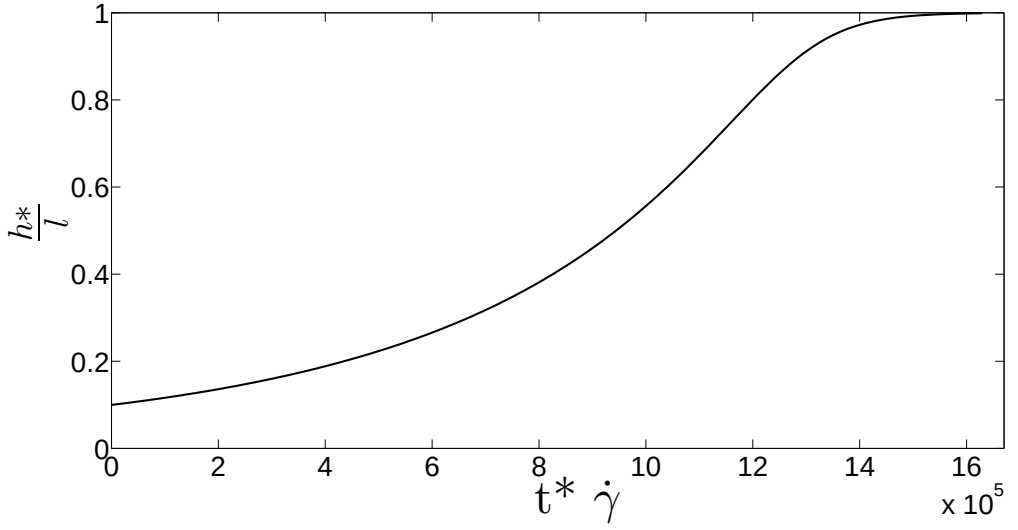

FIGURE 7. Trajectory of the fiber centre-of-mass for $\kappa = 100$ in a flow with Re=10^{-3} shown over a long period of time.

wall. The resulting evolution of the fiber centre of mass is,

$$\Delta h = -\cos\theta_m \Delta\theta \tag{3.13}$$

Here $\Delta\theta$ is the change of θ during a Jeffery orbit. This includes effects of both the inertial drift $\Delta\theta_{\hat{I}}$ and the wall contact $\Delta\theta_{\mathrm{N}}$. The perturbation to the fiber motion due to wall contact, captured through $\Delta\theta_{\mathrm{N}}$, can be obtained from equation (3.9) and (3.11) evaluated at $\phi = -\pi/2$. This leads to,

$$\frac{\Delta h}{\Delta\theta_{\mathrm{N}}} = -\frac{1+\sin^2\theta_m}{3\cos\theta_m} \tag{3.14}$$

The inertial perturbation to the quasi-steady Jeffery orbit between two consecutive wall contacts is found based on the change in C between $\phi = -\pi/2$ and $\pi/2$. To obtain this, first we consider the temporal evolution of C that accounts for the effects of finite inertia. This is given as,

$$\dot{C}_{\hat{I}} = \frac{\mathrm{Re}\,\mathrm{C}\epsilon'}{2} 2\sin^2\theta\sin^2\phi\cos^2\phi\left[\frac{1}{30} + \frac{\kappa^2}{\kappa^2\sin^2\phi+\cos^2\phi}\left[\frac{\cos^2\phi}{15} - \frac{\sin^2\phi}{6}\right]\right] \tag{3.15}$$

Integrating over $\phi = -\pi/2$ to $\pi/2$, which corresponds to motion over half of a Jeffery period gives the change in orbit constant, due to inertial effects, to be,

$$\Delta C_{\hat{I}} = \frac{\pi\mathrm{Re}\,\kappa\epsilon'\mathrm{C}}{30}\left[1 + \frac{2}{\kappa^2 C^2} - 2\sqrt{\frac{1}{\kappa^2C^2}+\frac{1}{\kappa^4C^4}}\right] \tag{3.16}$$

For slender fibers, the term, κC term is large except in a very small portion of orientation space that corresponds to orbits close to the flow-vorticity plane. These orientations only predominate when h is close to zero. Thus, we assume $\kappa C >> 1$ so that equation (3.16) reduces to,

$$\Delta C_{\hat{I}} = \frac{\pi\mathrm{Re}\,\kappa\epsilon'\mathrm{C}}{30} \tag{3.17}$$

To relate this to a perturbation in θ we take the derivative of equation (3.3) at $\phi = -\pi/2$.

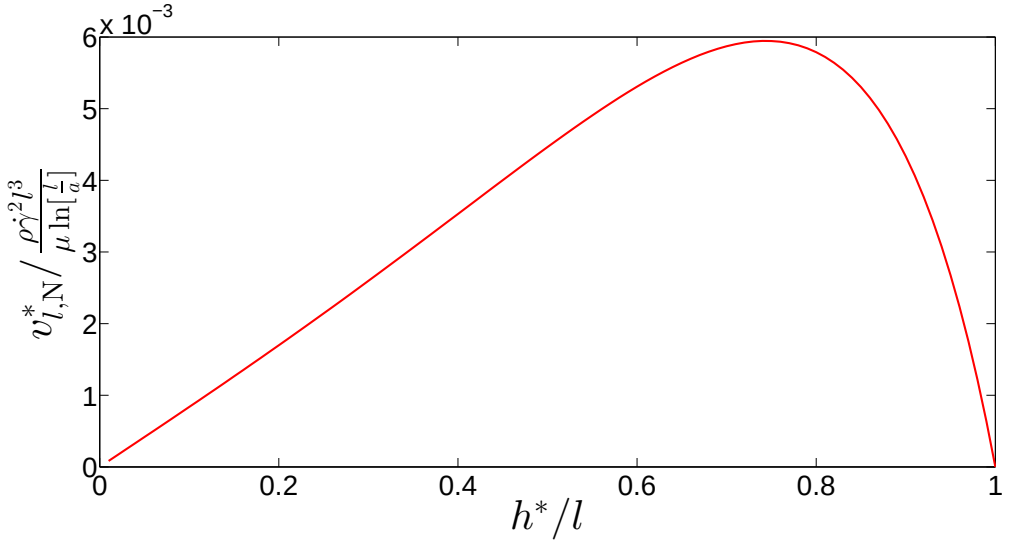

FIGURE 8. Lift velocity experienced by the fiber for $h < 1$

This gives,

$$\Delta\theta_{\hat{I}} = \cos^2\theta_m \Delta C_{\hat{I}} \tag{3.18}$$

so that

$$\Delta\theta_{\hat{I}} = \frac{\pi \mathrm{Re}\,\kappa\epsilon' \sin\theta_\mathrm{m}\cos\theta_\mathrm{m}}{30} \tag{3.19}$$

We can now obtain the drift of the fiber in a half Jeffrey orbit through equation (3.13) and inputs from equation (3.14) and (3.19):

$$\Delta h = -\cos\theta_m \left[\frac{\pi \mathrm{Re}\,\kappa\epsilon' \sin\theta_\mathrm{m}\cos\theta_\mathrm{m}}{30} - \Delta h \frac{3\cos\theta_m}{1+\sin^2\theta_m}\right] \tag{3.20}$$

Solving for Δh and dividing by the Jeffrey half period ($\pi\kappa$) gives the lift velocity during wall contact as,

$$v_{l,\mathrm{N}}(h) = \frac{\mathrm{Re}\,\epsilon'}{30}\left[\frac{\sin\theta_m\cos^2\theta_m[1+\sin^2\theta_m]}{4-2\sin^2\theta_m}\right] \tag{3.21}$$

At wall contact and by extension throughout the Jeffery orbit, the height of the fiber is given as $\sin\theta_m = h$. Thus,

$$v_{l,\mathrm{N}}(h) = \frac{\mathrm{Re}\,\epsilon'}{30}\left[\frac{h-h^5}{4-2h^2}\right] \tag{3.22}$$

Next, we rationalize the scaling of the lift velocity with wall contacts. All velocities are driven by the shear velocity $\dot{\gamma}l$. However, the orientational drift that drives wall collisions is a finite Re effect caused by an $O(\epsilon')$ disturbance velocity field that is important only during the $O(\kappa^{-1})$ fraction of the time when the fiber is flipping, leading to an $O(\epsilon'\kappa^{-1}\mathrm{Re})$ factor. Thus, the scaling of the dimensional lift velocity $v^*_{l,\mathrm{N}}$ due to contact and inertial orientation drift is given as, $\rho\dot{\gamma}^2 l^3/(\mu \ln\left[\frac{l}{a}\right])$.

Figure 8 shows the variation of wall contact lift velocity as a function of the height of the centre of the fiber. The lift velocity is small near $h = 0$, because the fiber is confined to orbits close to the flow-vorticity plane where its fluid velocity disturbance

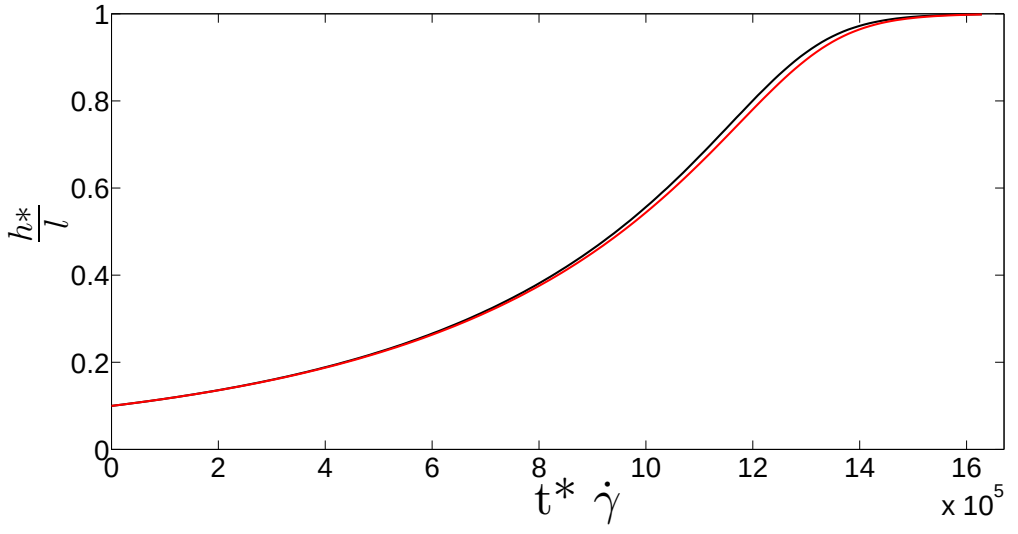

FIGURE 9. Comparison of the trajectory obtained from numerical simulation and the analytical model of lift velocity for $h < 1$. The model slightly under predicts the evolution.

and inertial rotation are small. The lift velocity grows approximately linearly with h until $h \approx 0.7$. Beyond this height, the change of orientation and lift velocity diminish as the fiber approaches the flow-gradient plane.

In figure 9 we compare the evolution of the centre of mass of the fiber obtained by tracking the trajectory with $\frac{dh^{\text{model}}}{dt} = v_{l,\text{N}}(h^{\text{model}})$. It can be seen that the model captures the change in position reasonably accurately. This confirms that at small Reynolds number, the constraint set by the accessible orbits that do not penetrate the wall captures the change of position obtained using a full description of the contact event.

The lift velocity presented in this section is driven by inertial drift of orientation and wall contact driven pole vaulting that breaks Stokes flow reversibility. This lift velocity is stronger by a factor of κ when compared to translation induced by inertia that was discussed in §2. So, to leading order, the direct effect of inertial drift of the centre of mass of the fiber does not contribute to wall contact lift velocity or the fiber dynamics in the $h < 1$ regime.

4. Discussion

In the previous sections we have discussed the behaviour of a fiber migrating away from a wall in shear flow in two regions: one where the fiber makes contact with the wall and one where it rotates freely in the shear flow. We now combine the results of the two previous sections and present the variation of lift velocity over the whole inner region $h^* \ll L_0$ as a function of the non-dimensionalised distance of the centre of the fiber from the wall in figure 10. In this plot the lift velocity is scaled as $\rho\dot{\gamma}^2 l^3/(\mu \ln\left[\frac{l}{a}\right])$ and is shown at various κ. The global peak of the scaled lift velocity occurs at $h < 1$ even at a moderate aspect ratio of 25. This is expected as the inertial lift force on a freely suspended fiber is weaker than the contact force driven by the inertial drift of orientation. This contact driven motion diminishes to zero due to the driving force becoming less and less effective as $h \to 1^-$. Thus, there is a thin $O(1/\kappa)$ region around $h \to 1^-$ where the fiber makes contact with the wall but the inertially induced translational velocity is

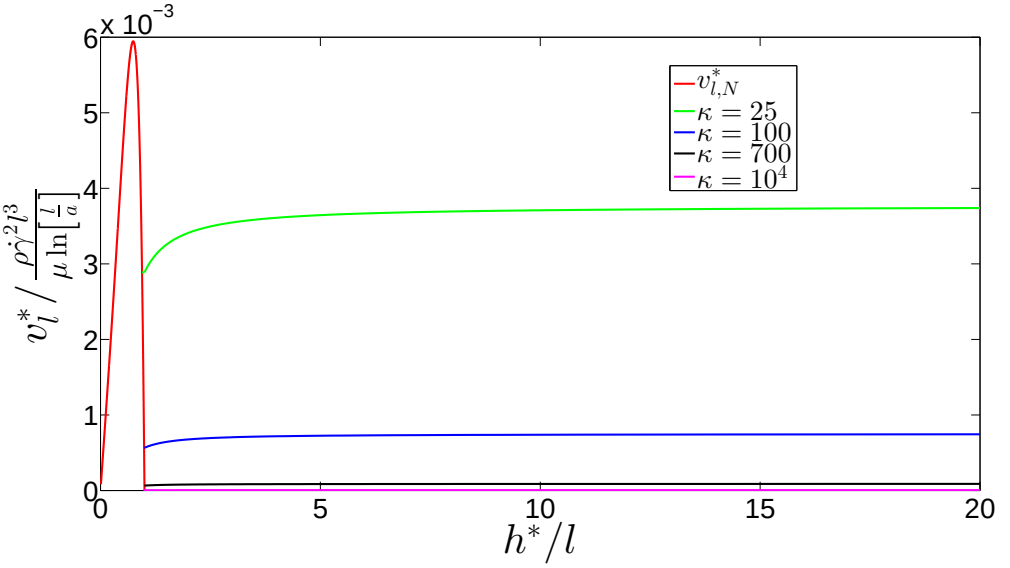

FIGURE 10. Variation of lift velocity v_l over the inner region, at aspect ratios of 25,100,700,10^4. For $h > 1$ the curves are in ascending order of aspect ratio going from top to bottom. For $h < 1$ the scaled velocity is independent of aspect ratio.

the dominant contributor to lift velocity. In figure 10, the lift velocity in this very small region is approximated by the value computed for $h \to 1^+$.

To complete the description of the manner in which the lift velocity varies with h, we briefly consider the lift velocity in the outer region $h^* \geqslant O(L_0)$. Although a detailed analysis of lift on a fiber has not been performed in this region, it can be noted that the qualitative dependence of the lift velocity on h is likely to be similar to that for spheres, because both can be viewed as point-force-dipoles on the length scale L_0, although the force dipole of a fiber varies periodically with time. McLaughlin (1993) showed that the lift force on a sphere has a maximum nearly equal to the large separation asymptote of the inner region, when $l \ll h^* \ll L_0$, and decays with wall separation in the outer region. It is reasonable to expect that the lift velocity of fibers exhibits a similar behaviour. Since the lift velocity maximum of the outer region corresponds to the inner region asymptote, it can be inferred that the maxima at $h \approx 0.7$ is likely to be the global maximum for high aspect ratio fibers while the value $0.03\rho\dot{\gamma}^2 l^2 a/(\mu \ln\left[\frac{2l}{a}\right])$ will be the global maximum lift velocity without wall contact.

One potential application of the result for the hydrodynamic lift on a fiber in wall-bounded shear flow is in cross-flow filtration. Cross-flow filtration is performed by flowing a suspension of particles through a channel or tube with a fluid filtrate drawn out through the porous walls. In conventional operation, the pores of the membrane block the passage of the particles, while transport processes in the channel including hydrodynamic lift, shear-induced hydrodynamic diffusion and molecular diffusion limit the accumulation of particles at the membrane surface (see Belfort *et al.* 1994; Altena & Belfort 1984). However, several investigators (see Hurwitz & Brantley 2000; Van Dinther *et al.* 2013; Masaeli *et al.* 2012) have suggested a sieve-free operation in which the pores are large enough to pass the particles but the transport in the channel prevents particles from flowing through the membrane with the filtrate. This mode of operation would have the advantage of reducing fouling and being less sensitive to colloidal interactions between the particles and the wall. The present results could facilitate design of sieve-free cross-flow

filtration based on lift where the separation accounts for the influences of particle shape as well as particle size. From the profile of the lift velocity as a function of h described above, one can determine the position at which particles would concentrate as a result of the balance of permeate and lift velocities. If the permeate velocity is sufficiently small, the particle will remain in the outer region $h^* > L_0$ far from the membrane. As the permeate velocity is increased, the wall separation of the fibers will decrease gradually until the permeate velocity reaches the value $0.0303\rho\dot{\gamma}^2 l^2 a/(\mu \ln\left[\frac{2l}{a}\right])$ corresponding to the maximum lift velocity occurring in the matching region $l \ll h^* \ll L_0$. When the permeate velocity exceeds this value, the fiber position will jump to a position near $h = 1$ in which the fiber makes contact with the wall. The permeate velocity could then be increased to substantially higher values but the retention of the fibers in the channel would depend on the details of the collisions of fibers with a porous boundary. The degree to which spherical particles can be retained in a porous channel due to their excluded volume interactions with the wall has been studied theoretically by Yan *et al.* (1991) and experimentally by Van Dinther *et al.* (2013), but no comparable analysis has yet been performed for non-spherical particles.

5. Conclusions

We have studied the hydrodynamic lift velocity of a neutrally buoyant fiber in the presence of a wall at small, but finite, Reynolds number. While the lift of spheres has been studied extensively, this is the first analytical study of the lift on non-spherical, neutrally buoyant particles in wall-bounded shear flow. The disturbance fluid velocity that generates lift is dominated by viscous effects provided that $h^* < L_0$. Thus the lift due to inertial effects can be obtained as a regular perturbation of the Navier-Stokes equation in terms of Reynolds number. The lift velocity has a strong dependence on geometry. The non-sphericity allows for wall contact and the fiber's lift velocity, when $a < h^* < l$, is dominated by its interactions with the wall. An equivalent case does not exist for a sphere.

For the freely rotating fiber with $h^* > l$, the lift velocity arises from the asymmetry of the flow around the fiber induced by inertial effects. In §2, we used a generalized reciprocal theorem to capture the first effects of inertia on the fiber velocity in terms of integrals involving the Stokes velocity field of a fiber in wall-bounded shear flow and a Stokes comparison problem with a fiber experiencing a force normal to the wall. The force distribution on the fiber was evaluated using slender-body theory and retaining non-dimensional forces per unit length of the fiber of $O(\frac{1}{\ln 2\kappa})$ and $O(\frac{1}{[\ln 2\kappa]^2})$. The boundary conditions on the wall were satisfied using the wall reflection image singularities associated with a Stokeslet as determined by Blake & Chwang (1974). The retention of $O(\frac{1}{[\ln 2\kappa]^2})$ forces is required to obtain quantitatively accurate predictions even for aspect ratios as high as 10^4. Terms of this order also capture a number of qualitative features that are not present at $O(\frac{1}{\ln 2\kappa})$ including a complex interaction of the fiber geometry with the imposed shear flow, the modification of the fiber force distribution due to wall interactions, and the oscillatory motion of the fiber perpendicular to the wall.

While the lift velocity of a sphere depends only on its distance from the wall, the lift velocity of a fiber depends on the wall separation as well as the fiber orientation. The force distribution on a fiber, driving the lift velocity, changes as it rotates in the shear flow. The temporal dynamics thus become important and are captured by Jeffery orbits. In particular, the Jeffery orbit $C = \infty$, corresponding to rotation in the flow-gradient plane, was shown by Subramanian & Koch (2005) to be the preferred configuration when fluid

inertia is present. A high aspect ratio fiber spends most of its time nearly aligned with the flow direction making a very small fluid velocity disturbance and an $O(\kappa^{-1})$ fraction of its orbit rotating through other orientations where it makes a larger disturbance. This behaviour causes the time averaged lift velocity to be a factor of κ^{-1} smaller than the value for a sphere with the same maximum dimension. The fiber lift velocity is reduced further by a factor of $\frac{1}{\ln 2\kappa}$ due to the small magnitude of the velocity disturbance of a slender body even when its axis has a substantial projection along the extensional axis of the imposed flow. These two factors cause the fiber lift velocity to have a non-trivial scaling with its half-length l and radius a and to reach a maximum value, for $l \ll h^* \ll L_0$, of $0.0303\rho\dot{\gamma}^2 l^2 a/(\mu \ln\left[\frac{2l}{a}\right])$ in contrast to the simpler result of $0.1\rho\dot{\gamma}^2 a^3/\mu$ for a sphere. A further qualitative difference between the lift velocity of a fiber and a sphere is that the lift velocity of a fiber changes by only a small amount as $h^* \to l$ while the lift velocity of a sphere vanishes as $h^* \to a$. This difference arises because the hydrodynamic resistance to translation of the fiber normal to the wall remains finite because of its thin cross-section and sharp edges while the lubrication resistance to normal motion of the sphere diverges.

Our study in §3 is the first to analyze the coupled effects of fluid-inertia induced orientational changes and pole vaulting of fibers due to wall contact. The solid-body contact between the fiber and wall pushes the fiber away from the wall and, if it is out of the flow-gradient plane, to an orbit further out of the plane. Inertial drift tends to bring the fiber to an orbit closer to the flow-gradient plane. The interplay of these two effects can be modelled as causing the fiber to drift across a sequence of quasi-steady orbits producing a net lift velocity. A detailed simulation of the orientational and translational trajectory of a fiber during wall contact was shown to be in good agreement with a model trajectory based on the quasi-steady orbit approximation. The scaling of the lift velocity due to wall contacts for $a < h^* < l$ was found to be $\rho\dot{\gamma}^2 l^3/(\mu \ln\left[\frac{l}{a}\right])$ which is larger than the case for no wall contact by a factor of the aspect ratio. This analytically derived lift velocity showed an initial increase which is almost linear with distance from the wall, then reached a maximum of about $0.006\rho\dot{\gamma}^2 l^3/(\mu \ln[\frac{l}{a}])$ and decreased to zero as $h \to 1$. This maximum was shown to be the global maximum even for fibers of moderate κ in §4.

The lift velocity finds application in industrial processes such as cross-flow filtration and laboratory processes including micro-fluidic separation. In §4 we have briefly described how knowledge of the lift velocity can be used to better control particles being filtered from the flow channel. In cross-flow filtration the results can be used to design a separation based on shape as well as size and one that does not rely upon the detailed interaction of the particles with the porous membrane. Criteria were derived for the shear rate and permeate velocity range which retains particles within the bulk of the channel as well as a range that leads to pole vaulting on the membrane surface. These criteria make a distinction based on geometry and will be useful in many industrial and laboratories systems where the filtrate is not spherical.

Acknowledgement

This work was supported by NSF-CBET grant 1505795.

REFERENCES

Altena, FW & Belfort, G 1984 Lateral migration of spherical particles in porous flow channels: application to membrane filtration. *Chemical Engineering Science* **39** (2), 343–355.

Batchelor, GK 1970 Slender-body theory for particles of arbitrary cross-section in stokes flow. *Journal of Fluid Mechanics* **44** (3), 419–440.

Belfort, Georges, Davis, Robert H & Zydney, Andrew L 1994 The behavior of suspensions and macromolecular solutions in crossflow microfiltration. *Journal of Membrane Science* **96** (1-2), 1–58.

Blake, JR & Chwang, AT 1974 Fundamental singularities of viscous flow. *Journal of Engineering Mathematics* **8** (1), 23–29.

Brenner, Howard 1961 The slow motion of a sphere through a viscous fluid towards a plane surface. *Chemical engineering science* **16** (3), 242–251.

Cherukat, Pradeep & McLaughlin, John B 1994 The inertial lift on a rigid sphere in a linear shear flow field near a flat wall. *Journal of Fluid Mechanics* **263**, 1–18.

Cox, Raymond G & Brenner, Howard 1967 The slow motion of a sphere through a viscous fluid towards a plane surface—ii small gap widths, including inertial effects. *Chemical Engineering Science* **22** (12), 1753–1777.

Dabade, Vivekanand, Marath, Navaneeth K & Subramanian, Ganesh 2016 The effect of inertia on the orientation dynamics of anisotropic particles in simple shear flow. *Journal of Fluid Mechanics* **791**, 631–703.

Drew, Donald A 1988 The lift force on a small sphere in the presence of a wall. *Chemical engineering science* **43** (4), 769–773.

Drew, Donald A, Schonberg, Jeffrey A & Belfort, Georges 1991 Lateral inertial migration of a small sphere in fast laminar flow through a membrane duct. *Chemical engineering science* **46** (12), 3219–3224.

Einarsson, Jonas, Candelier, F, Lundell, Fredrik, Angilella, JR & Mehlig, B 2015*a* Effect of weak fluid inertia upon jeffery orbits. *Physical Review E* **91** (4), 041002.

Einarsson, J, Candelier, F, Lundell, Fredrik, Angilella, JR & Mehlig, B 2015*b* Rotation of a spheroid in a simple shear at small reynolds number. *Physics of Fluids* **27** (6), 063301.

Feng, J, Hu, HH & Joseph, DD 1994 Direct simulation of initial value problems for the motion of solid bodies in a newtonian fluid. part 2. couette and poiseuille flows. *Journal of fluid mechanics* **277** (271), 271–301.

Harlen, Oliver G, Sundararajakumar, RR & Koch, Donald L 1999 Numerical simulations of a sphere settling through a suspension of neutrally buoyant fibres. *Journal of Fluid Mechanics* **388**, 355–388.

Harper, EY & Chang, I-Dee 1968 Maximum dissipation resulting from lift in a slow viscous shear flow. *Journal of Fluid Mechanics* **33** (2), 209–225.

Hurwitz, Mark F & Brantley, John D 2000 Shear separation: a promising method for protein fractionation. *Le Lait* **80** (1), 121–127.

Jayageeth, C, Sharma, Vivek Inder & Singh, Anugrah 2009 Dynamics of short fiber suspensions in bounded shear flow. *International Journal of Multiphase Flow* **35** (3), 261–269.

Jeffery, George B 1922 The motion of ellipsoidal particles immersed in a viscous fluid. In *Proceedings of the Royal Society of London A: Mathematical, Physical and Engineering Sciences*, , vol. 102, pp. 161–179. The Royal Society.

Khayat, RE & Cox, RG 1989 Inertia effects on the motion of long slender bodies. *Journal of Fluid Mechanics* **209**, 435–462.

Ku, Xiaoke & Lin, Jianzhong 2009 Effect of two bounding walls on the rotational motion of a fiber in the simple shear flow. *Fibers and Polymers* **10** (3), 302–309.

Lovalenti, Phillip M & Brady, John F 1993 The hydrodynamic force on a rigid particle undergoing arbitrary time-dependent motion at small reynolds number. *Journal of Fluid Mechanics* **256**, 561–605.

Marath, Navaneeth K & Subramanian, Ganesh 2017 The effect of inertia on the time period of rotation of an anisotropic particle in simple shear flow. *Journal of Fluid Mechanics* **830**, 165–210.

Masaeli, Mahdokht, Sollier, Elodie, Amini, Hamed, Mao, Wenbin, Camacho, Kathryn, Doshi, Nishit, Mitragotri, Samir, Alexeev, Alexander & Di Carlo, Dino 2012 Continuous inertial focusing and separation of particles by shape. *Physical Review X* **2** (3), 031017.

McLaughlin, John B 1991 Inertial migration of a small sphere in linear shear flows. *Journal of Fluid Mechanics* **224**, 261–274.

McLaughlin, John B 1993 The lift on a small sphere in wall-bounded linear shear flows. *Journal of Fluid Mechanics* **246**, 249–265.

Moses, Kelli B, Advani, Suresh G & Reinhardt, Andreas 2001 Investigation of fiber motion near solid boundaries in simple shear flow. *Rheologica acta* **40** (3), 296–306.

Nagel, Mathias, Brun, P-T, Berthet, Helene, Lindner, Anke, Gallaire, François & Duprat, Camille 2018 Oscillations of confined fibres transported in microchannels. *Journal of Fluid Mechanics* **835**, 444–470.

Qi, Dewei 1999 Lattice-boltzmann simulations of particles in non-zero-reynolds-number flows. *Journal of Fluid Mechanics* **385**, 41–62.

Saffman, PGT 1965 The lift on a small sphere in a slow shear flow. *Journal of fluid mechanics* **22** (02), 385–400.

Scheuer, A, Abisset-Chavanne, E, Chinesta, F & Keunings, R 2016 Second-gradient modelling of orientation development and rheology of dilute confined suspensions. *Journal of Non-Newtonian Fluid Mechanics* **237**, 54–64.

Shin, Mansoo, Koch, Donald L & Subramanian, Ganesh 2009 Structure and dynamics of dilute suspensions of finite-reynolds-number settling fibers. *Physics of Fluids (1994-present)* **21** (12), 123304.

Stover, Carl A & Cohen, C 1990 The motion of rodlike particles in the pressure-driven flow between two flat plates. *Rheologica Acta* **29** (3), 192–203.

Subramanian, G & Koch, Donald L 2005 Inertial effects on fibre motion in simple shear flow. *Journal of Fluid Mechanics* **535**, 383–414.

Van Dinther, AMC, Schroën, CGPH, Imhof, A, Vollebregt, HM & Boom, RM 2013 Flow-induced particle migration in microchannels for improved microfiltration processes. *Microfluidics and nanofluidics* **15** (4), 451–465.

Yan, Zong-Yi, Acrivos, Andreas & Weinbaum, Sheldon 1991 Fluid skimming and particle entrainment into a small circular side pore. *Journal of Fluid Mechanics* **229**, 1–27.

Yang, Seung-Man & Leal, L Gary 1984 Particle motion in stokes flow near a plane fluid–fluid interface. part 2. linear shear and axisymmetric straining flows. *Journal of Fluid Mechanics* **149**, 275–304.